CONFERÊNCIA NACIONAL DE MÉTODOS NUMÉRICOS EM
MECÂNICA DOS FLUIDOS E TERMODINÂMICA 2006
FCT-UNL, Monte de Caparica, 8 e 9 de Junho, 2006

APPLICATION OF THE LOG-CONFORMATION TENSOR APPROACH TO FINITE-VOLUME PREDICTIONS OF VISCOELASTIC FLOWS

Alexandre M. Afonso[1,2], Manuel A. Alves[2]*, Fernando T. Pinho[1,3] and Paulo J. Oliveira[4]

1: Universidade do Minho,
Largo do Paço, 4704-553 Braga,
e-mail: fpinho@dem.uminho.pt, web: http://www.uminho.pt

2: Departamento de Eng. Química, CEFT,
Faculdade de Engenharia da Universidade do Porto
Rua Dr. Roberto Frias, 4200-465 Porto, Portugal
e-mail: mmalves@fe.up.pt, web: http://www.fe.up.pt

3: Centro de Estudos de Fenómenos de Transporte,
Faculdade de Engenharia da Universidade do Porto
Rua Dr. Roberto Frias, 4200-465 Porto, Portugal
e-mail: aafonso@fe.up.pt, fpinho@fe.up.pt, web: http://www.fe.up.pt

4: Departamento de Eng. Electromecânica
Universidade da Beira Interior
6201-001 Covilhã, Portugal
e-mail: pjpo@ubi.pt, web: http://www.ubi.pt

Keywords: Plane contraction; Viscoelastic; Log-conformation tensor; Finite-volume.

Abstract. *A finite-volume method is applied to the numerical simulation of laminar viscoelastic flows through a planar 4:1 abrupt contraction. The calculation of the polymer stress contribution is carried out with the log-conformation methodology recently proposed by Fattal and Kupferman [1]. This approach, never used before in the context of a finite volume method, neither with the UCM nor Oldroyd-B models in this particular geometry, was not able to overcome the High Weissenberg Number Problem (HWNP) in contrast to the other works where it used with globally stable differential constitutive equations [1-5], due to the onset of a natural elastic instability.*

1 INTRODUCTION

A finite-volume method (FVM) is applied to the numerical simulation of laminar viscoelastic flows through a planar 4:1 abrupt contraction. The upper-convected Maxwell (UCM) and Oldroyd-B fluids (Old-B) [6,7], were selected for this study, in order to allow direct

comparison with previous works by Oliveira and Pinho [8] and Alves et al [9,10], and also to analyse the applicability of the matrix logarithm formalism for Maxwell-type models in a flow with geometric singularities.

It is well known that geometries with singularities, like contraction flows, pose a great challenge to numerical methods, especially at high Deborah numbers (a measure of the elasticity of the flow). The planar 4:1 sudden contraction is a benchmark geometry since the Fifth International Workshop on Numerical Methods in Non-Newtonian Flows in 1987 [11]. Owens and Phillips [12], McKinley et al. [13] and Boger [14] present extensive literature reviews on experiments in this flow.

A wealth of numerical research has also been done, especially for the axisymmetric geometry. Extensive reviews of numerical investigations on both axisymmetric and planar contractions can be found in Keunings [15], Baaijens [16], Walters and Webster [17], Owens and Phillips [12] and Oliveira and Pinho [8]. This has been more recently complemented by a review on square 3D contraction flows in the visualization work of Alves et al [18] in a 4:1 square–square contraction using Boger fluids.

Alves et al [9] have used high order spatial discretization schemes and fine meshes to predict accurately the flow of UCM fluids in the 4:1 planar contraction, thus improving on earlier predictions of Oliveira and Pinho [8]. Subsequently, Alves et al. [10] used a new convection scheme (CUBISTA) with the Oldroyd-B fluid, achieving convergence up to De=2.5 on their finest mesh. The results presented were cloese to those obtained by Aboubacar et al. [19] with a hybrid finite volume/element scheme. The results obtained by Kim et al [20] in the same geometry with an Oldroyd-B model were also very close to those of Alves et al [10]. Kim et al [20] used a transient numerical algorithm based on the four-step fractional step method and DEVSS-G/DG with equal-order linear interpolation functions and also obtained converged solutions up to De=2.5 with their finest mesh. Recently, the benchmark results of Alves et al [10] were also confirmed by Belblidia et al [21], in their steady-state investigation with the Oldroyd-B model using different stabilisation methodologies embedded within a time-marching incremental pressure-correction formulation.

In this work we have implemented the methodology recently proposed by Fattal and Kupferman [1], the so colled matrix-logarithm or log-conformation formulation (denomination used heretoforth) of the viscoelastic constitutive equations, which is based on a reformulation of the constitutive law in terms of the matrix logarithm of the conformation tensor. According to their authors, this new formulation introduces a better polynomial interpolation of the logarithm of the variables that exhibit an exponential growth near stagnation points and also preserves the positive definiteness of the conformation tensor [1-5]. Fattal and Kupferman [1] also reported a breakthrough in the High Weissenberg Number Problem (HWNP; like the Deborah number, the Weissenberg number measures the flow elasticity) in their numerical simulations with the finitely-extensible nonlinear elastic (FENE) Chilcott–Rallison model in a two-dimensional lid-driven cavity flow. Later, Fattal and Kupferman [2] applied the log-conformation scheme to an Oldroyd-B fluid in the same geometry, using a multigrid solver and gave an explanation for the high Weissenberg number *instability* phenomenon, indicaing the possibility to perform stable simulations at very large

values of the Weissenberg number. They included a stability condition and stated that it may be very restrictive when convection is weak, as in creeping flows, and in the presence of large deformation rates, as in the flow around sharp corners.
Hulsen et al [3] made the first implementation of the log-conformation methodology with a finite element method (FEM) and applied it to the benchmark flow of Oldroyd-B and Giesekus fluids past a confined cylinder. This work reported an almost unbounded convergence limit for the Giesekus model, whereas for the Oldroyd-B the solution became unsteady at high Deborah numbers while exhibiting symptoms of mesh dependency.
Kwon [4] has numerically investigated the planar 4:1 contraction flow with the Leonov constitutive equation and found more stable computations when using the log-conformation method than with the conventional approach. Kwon [4] has also concluded that this new method may only work for constitutive equations that are proven globally stable and that the stability constraint has to be taken into serious consideration. In a sequel, Yoon and Kwon [5] obtained solutions for Deborah numbers in excess of 100 using finer meshes. These authors also presented solutions for the 4:1:4 contraction/expansion flow and obtained converged solutions for Deborah numbers higher than 10. In both geometries, the convergence limits decreased with mesh refinement.
The remainder of this paper is organised as follows: after presenting the governing equations the log-conformation modified constitutive equation is described. Then, we introduce a set of parameters used in this work to classify the flow and help analyse the loss of evolution phenomenon. Prior to the presentation of results we briefly describe the numerical method and present the geometry and computational meshes.

2 GOVERNING EQUATIONS

To simulate the steady incompressible flow of viscoelastic fluids, the following set of governing equations needs to be solved: conservation of mass,

$$\nabla \cdot \mathbf{u} = 0\,, \tag{1}$$

conservation of momentum (creeping flow):

$$\rho \frac{D\mathbf{u}}{Dt} = -\nabla p + \beta \eta_o \nabla \cdot \left(\nabla \mathbf{u} + \nabla \mathbf{u}^T\right) + \frac{\eta_o}{\lambda}(1-\beta)\nabla \cdot \mathbf{A}\,, \tag{2}$$

and a constitutive equation describing the evolution of the conformation tensor, **A**,

$$\mathbf{A} + \lambda \overset{\nabla}{\mathbf{A}} = \mathbf{I} \tag{3}$$

where $\overset{\nabla}{\mathbf{A}}$ represents Oldroyd's upper convected derivative of **A**, **I** is the unit tensor, **u** is the velocity vector, p is the pressure and λ is the relaxation time of the polymer. The viscosity ratio is β defined as the ratio between the Newtonian solvent viscosity, η_s, and the total zero shear rate viscosity,

$$\beta \equiv \frac{\eta_s}{\eta_o} = \frac{\eta_s}{\eta_s + \eta_P} \tag{4}$$

and it allows selection from the two quasi-linear constitutive models used in this work: if $\beta = 0$ then the system of equations (2-3) defines the upper-convected Maxwell (UCM) fluid and if $0 < \beta < 1$ the Oldroyd-B model [6,7]. The value of parameter β is taken to be 1/9 throughout this work, a standard value used in computational rheology. The constitutive law written in terms of the conformation tensor **A**, can be explicitly formulated as a function of the polymer contribution to the extra stress tensor, $\boldsymbol{\tau}$, with the following relation valid for both models,

$$\boldsymbol{\tau} = \frac{\eta_p}{\lambda}\left(\mathbf{A} - \mathbf{I}\right) \tag{5}$$

and thus, the system of the governing equations can be written explicitly in terms of the extra stress tensor. Such formulation was followed in past works with our simulation code [8-10,18,28,29,31] but is not convenient now.

2.1 The *log-conformation* representation

As mentioned above, Fattal and Kupferman [1] suggested a simple tensor-logarithmic transformation of the conformation tensor for differential viscoelastic constitutive equations, which includes a significant number of constitutive laws for possible application of the matrix-logarithm. The core feature of the transformation is the decomposition of the velocity gradient, $\nabla \mathbf{u}$, into a traceless extensional component, **E**, and a pure rotational component, **R**. With this decomposition, the constitutive law in equation (3), can be re-written as [1]

$$\frac{\partial \mathbf{A}}{\partial t} + (\mathbf{u}.\nabla)\mathbf{A} - \left(\mathbf{RA} - \mathbf{AR}\right) - 2\mathbf{EA} = \frac{1}{\lambda}\left(\mathbf{I} - \mathbf{A}\right), \tag{6}$$

In the *log-conformation* representation equation (6) is replaced by an equivalent equation for the logarithm of the conformation tensor, $\boldsymbol{\Theta} = \log \mathbf{A}$, benefiting from the fact that **A** is a symmetric positive definite (SPD) matrix, and thus can always be diagonalized into the form:

$$\mathbf{A} = \boldsymbol{\Omega}\mathbf{D}\boldsymbol{\Omega}^T = \boldsymbol{\Omega}^T\mathbf{D}\boldsymbol{\Omega}, \tag{7}$$

where $\boldsymbol{\Omega}$ is an orthogonal matrix made with the eigenvectors of matrix **A** and **D** is a diagonal matrix made with the corresponding three distinct eigenvalues of matrix **A**. The change from equation (6) to an equation for $\boldsymbol{\Theta} = \log \mathbf{A}$ is straightforward, and leads to [1]

$$\frac{\partial \boldsymbol{\Theta}}{\partial t} + (\mathbf{u}.\nabla)\boldsymbol{\Theta} - \left(\mathbf{R}\boldsymbol{\Theta} - \boldsymbol{\Theta}\mathbf{R}\right) - 2\mathbf{E} = \frac{e^{-\boldsymbol{\Theta}}}{\lambda}\left(\mathbf{I} - e^{\boldsymbol{\Theta}}\right) = \frac{1}{\lambda}\left(e^{-\boldsymbol{\Theta}} - \mathbf{I}\right), \tag{8}$$

2.2 Loss of evolution and flow classification

The positive definiteness of the conformation tensor is known to be crucial for well posedness of the evolution equation, although some degree of loss of evolution may be found in constitutive equations that have been proven to be stable under short and high frequency wave disturbances (Hadamard stability, Dupret and Marchal [22] and Lee *et al* [23]).
In this work we used two different stability criteria. One is simply to examine whether the determinant of the conformation tensor is positive ($\det \mathbf{A} > 0$), because if it is non postive, the positive definiteness of **A** tensor is violated. The other criterion for judging the performance of the numerical descritization is to determine if the elastic tensor:

$$\mathbf{T} = \boldsymbol{\tau} + \frac{\eta_P}{\lambda}\mathbf{I} = \frac{\eta_P}{\lambda}\mathbf{A}\,, \tag{9}$$

is positive definite (Dupret and Marchal [22]). The matrix is said to be positive definite when all the eigenvalues are positive, and this is quantified by the system condition number, *S*, used to indicate temporal loss of evolution [20] (for 2D flow):

$$S = 2\frac{\lambda_1\lambda_2}{\lambda_1^2 + \lambda_2^2} = 2\frac{\det \mathbf{T}}{\mathrm{tr}(\mathbf{T}^2)}\,, \tag{10}$$

where λ_1 and λ_2 are the non trivial eigenvalues of the tensor **T**.
Another useful parameter used to analyse the results of the log conformation is related to a flow classification method valid only for plane flows. Here we adopt the normalized version of Astarita's [24] criterion, as proposed by Mompean et al [25],

$$D = \frac{1 - X}{1 + X}\,, \tag{11}$$

where X is Astarita's parameter. Scalar D varies between −1 and +1: for simple shear flow, D=0; for extensional flow, $D \rightarrow +1$ and as the flow approaches a rigid body motion, D tends to −1. This type of D-map utilization was also applied in planar contraction flow by Mompean et al [25] and Thompson et al [26], and more recently by Phelan et al [27] for complex geometries.

3 NUMERICAL METHOD

In the past, our group adapted a Newtonian finite-volume method (FVM) to calculate viscoelastic flows using various differential rheological constitutive equations for the polymer contribution to the extra stress tensor [8-10,18]. This fully-implicit FVM is based on a time marching pressure-correction algorithm, formulated with the collocated variable arrangement. A detailed explaination of the method can be found in Oliveira et al [28] and Alves et al [29]. Here, the method was extended to the *log-conformation* procedure and the corresponding modifications are explained below.
The governing equations are first transformed to a non-orthogonal system, but keeping the

Cartesian velocity and conformation/log-conformation components. The log-conformation tensor evolution equation can thus be written into a general non-orthogonal coordinate system ($\varsigma_1, \varsigma_2, \varsigma_3$),

$$\frac{\partial J\Theta_{ij}}{\partial t} + \frac{\partial}{\partial \varsigma_k}\left(u_k \beta_{lk} \Theta_{ij}\right) = J\left(R_{ik}\Theta_{kj} - \Theta_{ik}R_{kj}\right) + 2JE_{ij} + \frac{J}{\lambda}\left(e^{-\Theta_{ij}} - \delta_{ij}\right). \qquad (12)$$

After integration over the control volumes forming the computational mesh, and in time over a time step (δt), the β_{lk} coefficients are replaced by area components (index k) of the surface whose normal vector points towards direction l, the Jacobian J is replaced by the cell volume V, and the derivatives $\partial/\partial\varsigma_l$ become differences between values along direction l.
Then after the discretization, the various terms are assembled, obtaining

$$a_P^{\Theta}\Theta_{ij,P} - \sum_F a_F^{\Theta}\Theta_{ij,F} = S_{\Theta_{ij}} + \frac{\lambda_P V_P}{\delta t}\Theta_{ij,P}^0, \qquad (13)$$

where $\Theta_{ij,P}^0$ refers to the ij component of the log-conformation tensor at the previous time level, a_P^{Θ} represents the central coefficient, a_F^{Θ} represents the coefficients of the neighbouring cells (with F spanning the near-neighbouring cells of cell P) and $S_{\Theta_{ij}}$ is the total source term.
The discretised momentum equations are solved sequentially after assembling all coefficients and source terms, to obtain the three Cartesian velocity components u, v and w. As generally the velocity components do not satisfy the continuity equation a pressure-correction field, obtained from a Poisson pressure equation, is solved with a symmetric conjugate gradient method preconditioned with an incomplete LU decomposition.
The advective term in equation (8) was discretized with three distinct differencing schemes: the first-order accurate scheme UDS (upwind differencing scheme), the formally third-order accurate scheme QUICK (Quadratic Upstream Interpolation Scheme for Convective Kinematics) [30] and the high resolution scheme CUBISTA of Alves et al [29], formally of third-order accuracy and especially designed for differential constitutive relations.

4 FLOW GEOMETRY AND COMPUTATIONAL MESH

The flow geometry and boundary conditions are illustrated in **Figure 1**. Only half of the two dimensional domain is used for most of the computations, with symmetry conditions imposed at the centreline, y=0. However, at high Deborah numbers, some calculations are performed in the whole domain, so that flow instabilities can be predicted. The half-width of the downstream channel H_2 is taken as the characteristic length scale and the average velocity in that channel U_2 is the characteristic velocity scale. Stresses are normalised with T_w=3$\eta U_2/H_2$. We use an inlet length of L_1 =40H_2 and an outlet length L_2=100H_2, both

sufficient for complete flow development upstream and downstream of the contraction. Calculations with the UCM and Oldroyd-B models, at a constant vanishing Reynolds number $Re=\rho H_2 U_2/\eta=0$ (creeping flow), were carried out with three meshes M1, M2 and M3 (their major characteristics are listed in **Table 1**). Mesh M1C has the same characteristics of mesh M1 but covers the whole domain without relying on symmetry. The mesh data in **Table 1** lists the total number of control volumes in the meshes (*NC*), the number of degrees of freedom (*DOF*) and the minimum normalised mesh spacing in both directions. These computational meshes are orthogonal but non-uniform, and the concentration of cells is higher near the corner of the contraction and the walls (in such a way that $\Delta x_{min}= \Delta y_{min}$), where the conformation tensor gradients are expected to be higher. A view of the mesh M2 near the contraction plane is depicted in **Figure 1**.

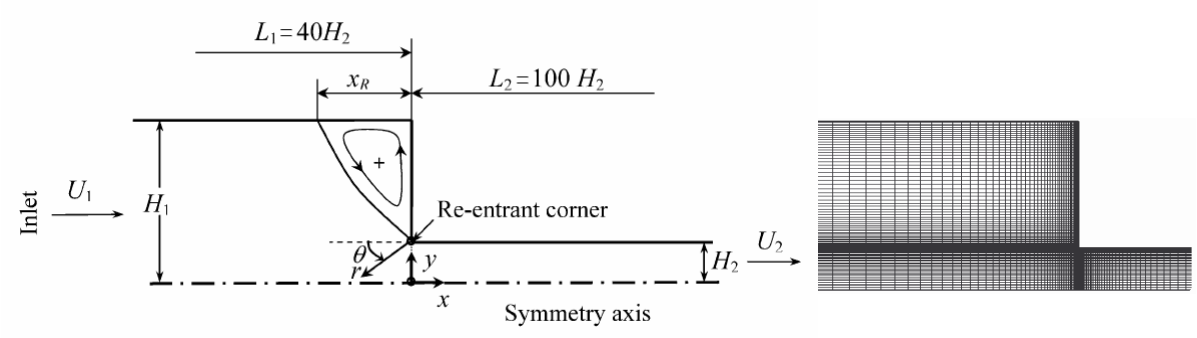

Figure 1. Schematic representation of the 4:1 contraction geometry (from [10]) and detailed view near the contraction plane in Mesh M2.

	Number of cells	Degrees of freedom	Δx_{min}; Δy_{min}
M1	5282	31692	0.020
M2	10587	63522	0.014
M3	42348	254088	0.0071
M1C	10562	63384	0.020

Table 1. Computational meshes.

In order to analyse the log-conformation formalism introduced earlier, all simulations were carried out in two different formulations: the standard formulation using the extra stress tensor (i.e. without using the conformation tensor) and the formulation using the log-conformation tensor (for conciseness henceforth denoted ***StrT*** and ***LogT***, respectively). In both formulations the $L_{2\text{-norm}}$ of the residuals of the equations was required to be less than a tolerance of 10^{-4}, in order to stop the time stepping procedure, and all the calculations were obtained with the same time step increment (Δt). Increments in the relaxation time of the fluid, λ, at a fixed average velocity, allows a direct increase of the Deborah number, here defined as

$$De = \frac{U_2 \lambda}{H_2} \tag{17}$$

In the next sections we present some qualitative (streamlines and flow classification) and quantitative results (length of primary vortex, distribution of the normalized first normal stress differences (N_1/T_w) along the centreline and downstream channel wall and stability criterions). The results are presented in the following sequence: in section 5.1 we present results for the UCM model and in section 5.2 the results for the Oldroyd-B fluid.

5. RESULTS

5.1 UCM model

Results for the length of the corner vortex (X_R) for both the *strT* and *LogT* formulations, obtained on meshes M1, M2 and M3 and with three different interpolating schemes for the convective terms in the constitutive equation (UDS, QUICK and CUBISTA) are presented in **Table 2** and in **Figure 2**.

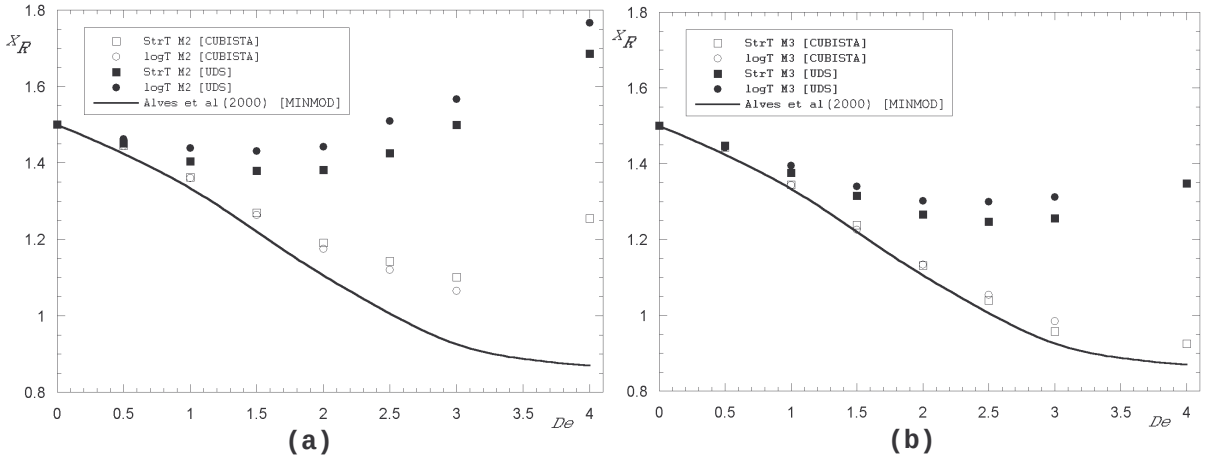

Figure 2. Dimensionless length of primary vortex as a function of Deborah number - UCM: (a) M2 (b) M3.

For Newtonian fluids, only the CUBISTA scheme was used and good convergence behaviour, independent of mesh refinement and formulation, was obtained. For the viscoelastic fluids the results obtained with the *strT* formulation follow the trends of previous works by Oliveira and Pinho [8] and Alves et al [9], with the length of the corner vortex decreasing with elasticity, measured by the Deborah number, up to a level of $De \approx 3$. Note that the finest mesh used in this work is less refined than that used by Alves et al [9] and here we used a different high resolution scheme. These differences are reflected in the slightly different value of X_R for $De \geq 3$. It was found that the QUICK scheme was stable only at moderate values of Deborah numbers with the *strT* formulation, due to its unbounded character. The influence of mesh refinement and interpolation scheme is also

the same reported in the last works (see **Figure 4**), with the upwind scheme introducing some numerical diffusion and the corner vortex length and intensity decreasing significantly with mesh refinement. Visually, **Figure 4** shows no difference between results with the *StrT* and *LogT* formulations.

		M1		M2		M3	
De	Scheme	***StrT***	***LogT***	***StrT***	***LogT***	***StrT***	***LogT***
0.0	Cubista	1.495	1.495	1.497	1.497	1.499	1.499
0.5	UDS	1.451	1.463	1.451	1.462	1.448	1.443
	Quick	1.446	1.446	1.445	1.444	1.442	1.440
	Cubista	1.446	1.447	1.446	1.445	1.443	1.442
1.0	UDS	1.422	1.462	1.404	1.439	1.376	1.395
	Quick	1.366	1.363	1.360	1.358	1.344	1.342
	Cubista	1.369	1.368	1.362	1.360	1.345	1.343
1.5	UDS	1.424	1.485	1.379	1.431	1.315	1.340
	Quick	1.287	1.289	1.261	1.271	*	1.232
	Cubista	1.295	1.288	1.270	1.264	1.238	1.226
2.0	UDS	1.463	1.542	1.382	1.442	1.266	1.302
	Quick	1.209	1.212	1.173	(1.185) [a]	*	b
	Cubista	1.231	1.249	1.191	1.175	1.131	(1.133) [a]
2.5	UDS	1.526	1.626	1.425	1.510	1.247	1.299
	Quick	1.170	(1.203) [a]	*	(1.138) [a]	*	b
	Cubista	1.210	1.186	1.143	(1.120) [a]	1.039	(1.064) [a]
3.0	UDS	1.621	1.680	1.499	1.567	1.256	(1.312) [a]
	Cubista	1.236	(1.199) [a]	1.101	(1.065) [a]	0.957	(0.984) [a]
4.0	UDS	1.836	1.893	1.686	1.766	1.348	b
	Cubista	1.334	b	1.255	b	0.925	b

* diverged; [a] – X_R oscillates with harmonic periodicity; b - X_R oscillates periodically.

Table 2. Dimensionless length of primary vortex (X_R) as a function of Deborah number, mesh, interpolating scheme and formulation.

However, closer inspection reveals that the *LogT* formulation captures an unsteady flow pattern that is absent in the *StrT* formulation. The vortex size follows the trend as in the *strT* formulation up to $De \approx 2$ in all meshes. At higher Deborah numbers and in refined meshes it starts to present a time dependent harmonic periodic oscillation. The values of X_R inside brackets in **Table 1** represent the average value of X_R corresponding to this harmonic oscillation, as the case reported in **Figure 3a**. This type of time-dependent behaviour, due to a pure elastic instability, has been observed in many experimental investigations (Boger et al. [14] and McKinley et al. [13]) and some numerical works (Oliveira [31] with the PTT and Giesekus models at high Deborah numbers, $De \approx 5$, and creeping flow conditions).

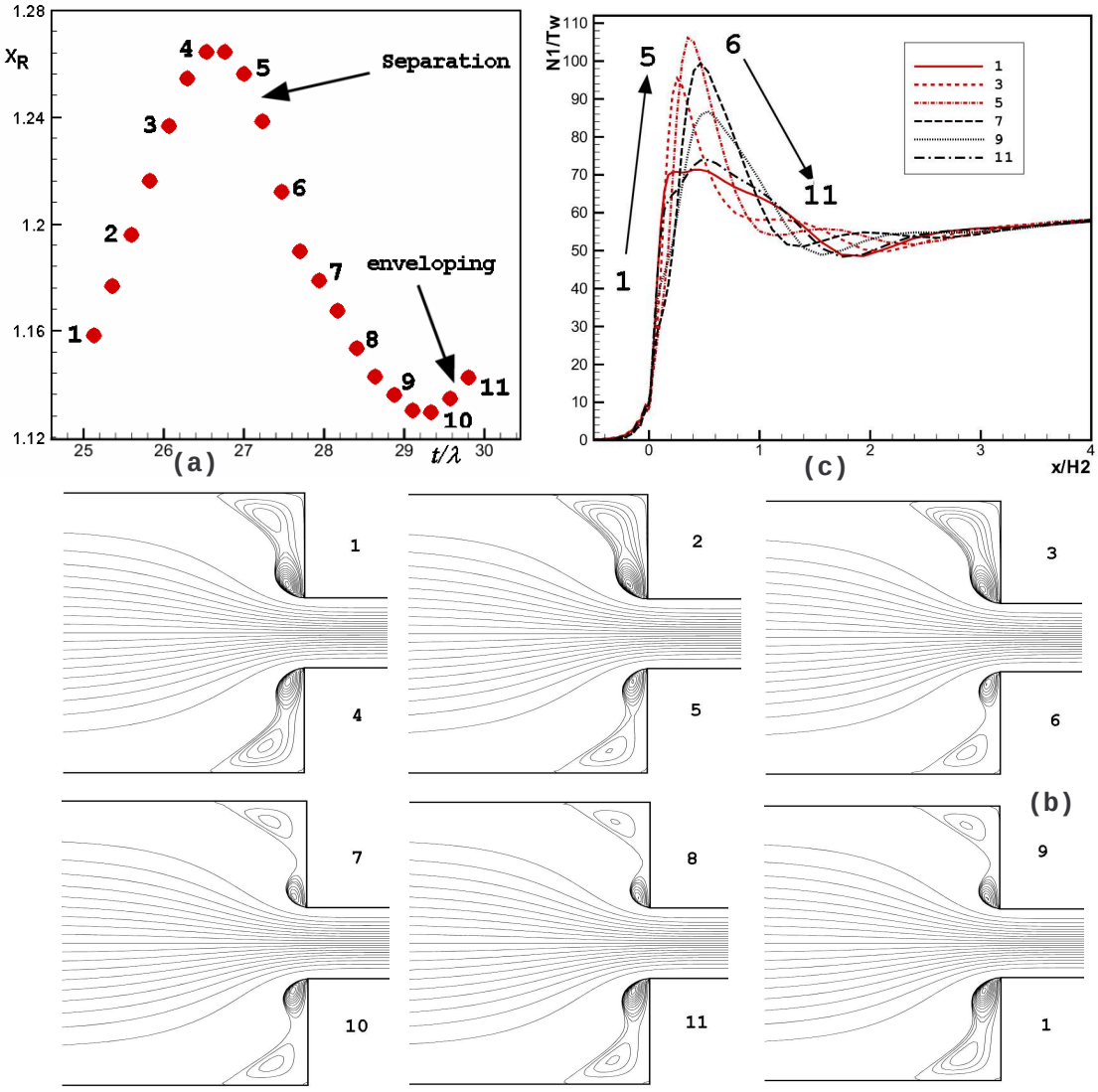

Figure 3. Harmonic periodically oscillations of vortical structures at De=3 for the UCM, using the CUBISTA scheme in mesh M1C. Note: $\Delta\Psi = 0.2 \times 10^{-3}$ in recirculations.

Whether this phenomenon is a natural unsteady feature of viscoelastic fluid flows in contractions or a numerical artifact requires further investigation using a time-dependent procedure instead of the pseudo-transient calculation which is not allowed to fully converge at each time step (in this method the inertial term is kept in the equations to advance in time acting as under-relaxation).

So far, some evidence corroborates the first hypothesis because the unsteadiness happens with all discretization schemes (hence, it is not a switching instability), both the minimum values of the system condition number, S_{min} and the $\det(\mathbf{A})_{min}$, are always positive, and finally it always starts near the reported critical Deborah numbers for this benchmark flow problem. We can also ask ourselves whether the Log conformation is capable of a better approach to

this flow problem.

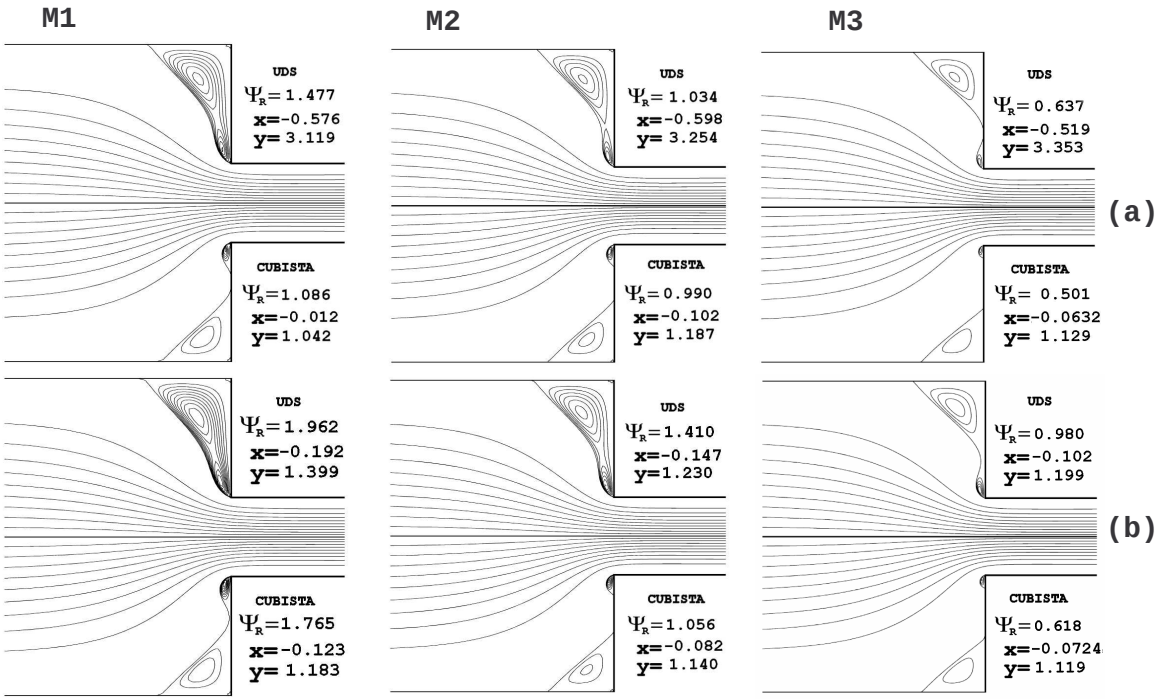

Figure 4. Coupled effect of mesh refinement and differencing scheme on the streamline patterns at De=2.0 for the UCM: (a) *strT*; (b) *LogT*. Note: $\Delta\Psi = 0.2 \times 10^{-3}$ in recirculations and Ψ_R multiplied by 10^3.

As the Deborah number is increased further the time dependent oscillations evolve from a periodic harmonic to a more complex behaviour. **Figure 3a** shows the evolution of X_R as a function of time for CUBISTA scheme at De=3 using mesh M1C (mesh M1 in the full domain) and *LogT*. In this simulation the number of time-steps per relaxation time of is of the order of 800. We note that a first-order implicit Euler scheme is used here for the time integration, and as such the time accuracy is low. Further studies, preferably with second-order schemes, will be done in the near future. **Figure 3b** presents stills taken along a period cycle of pulsation showing the merging process of the corner and lip vortices. Interesting is also the observation of the time variation of the normalized first normal stress difference (N_1/T_w) along the axial direction near the downstream duct wall shown in **Figure 3c**. The maximum value of N_1/T_w is reached just after the maximum extension of the bubble X_R (in the separation moment) and the minimum N_1/T_w occurs when the two vortices merge.

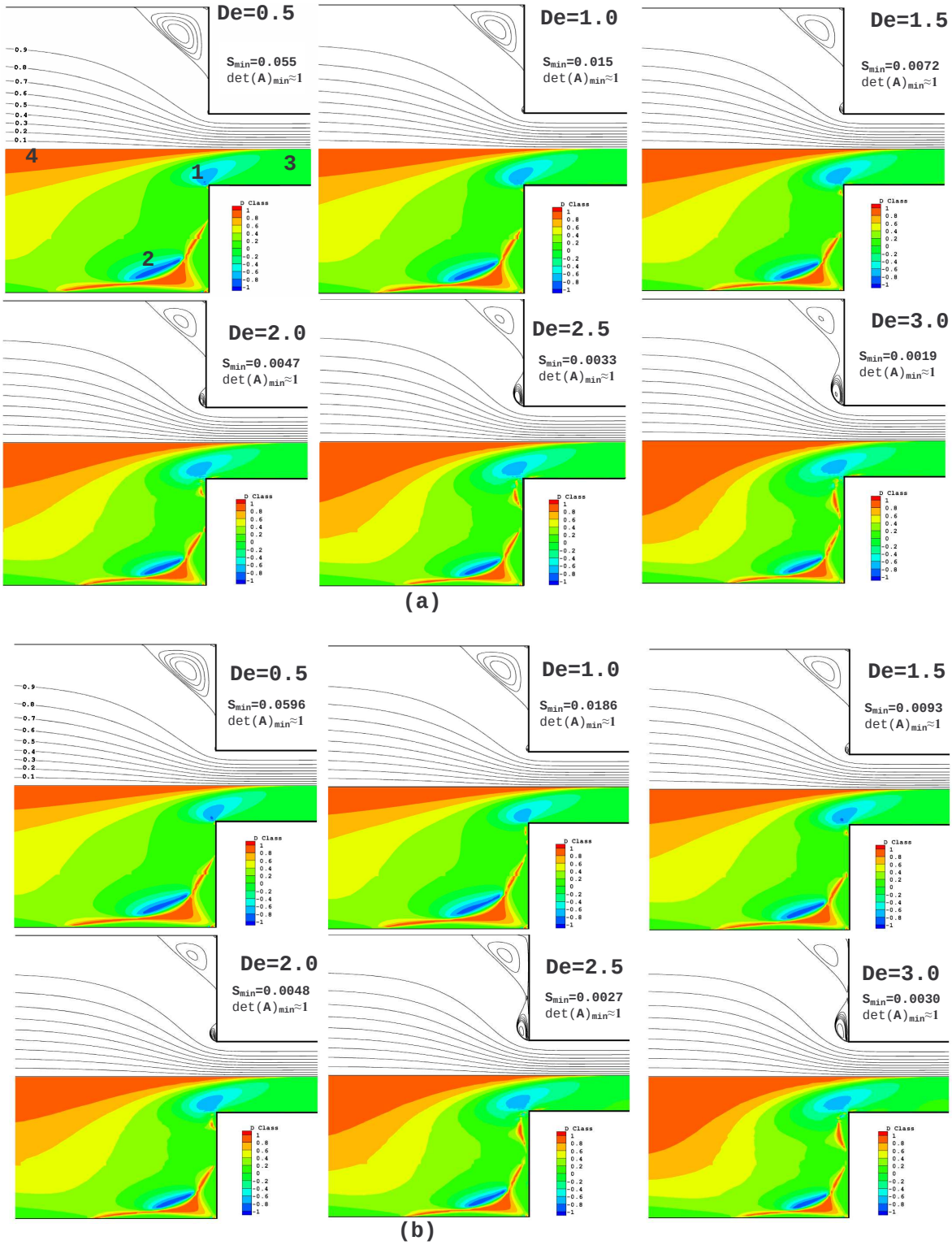

Figure 5. Flow patterns (top half) and Flow classification (bottom half) in mesh M2 for the UCM. (a) *strT*; (b) *LogT* [S_{min} and det(**A**)$_{min}$ – beside each map]

To assess whether this unsteady behaviour is also seen in the intensity of the recirculation of the corner vortex (defined by $\Psi_R = (\psi_R/U_1H_1)-1$) we compare in **Figure 4** streamlines pertaining to simulations with different meshes and for both methods of computation at at De=2. Even for the simulations with the *LogT* formulation, which at this lower value of De present no oscillations, we observe a different intensity relative to that calculated with the *strT* formulation. In the *strT* formulation and with both schemes, the eye of the recirculation is located at the same place and the maximum value of Ψ_R decreases with mesh refinement. In the *LogT* formulation with the CUBISTA scheme, all maximum values of Ψ_R decrease with mesh refinement, but they are always greater than those of *strT*. Note that no oscillations in the eddies were found in meshes M1 and M2 at this Deborah number. With the UDS scheme, the maximum Ψ_R values are always larger than those obtained with CUBISTA for both formulations, a clear sign of excessive numerical diffusion.

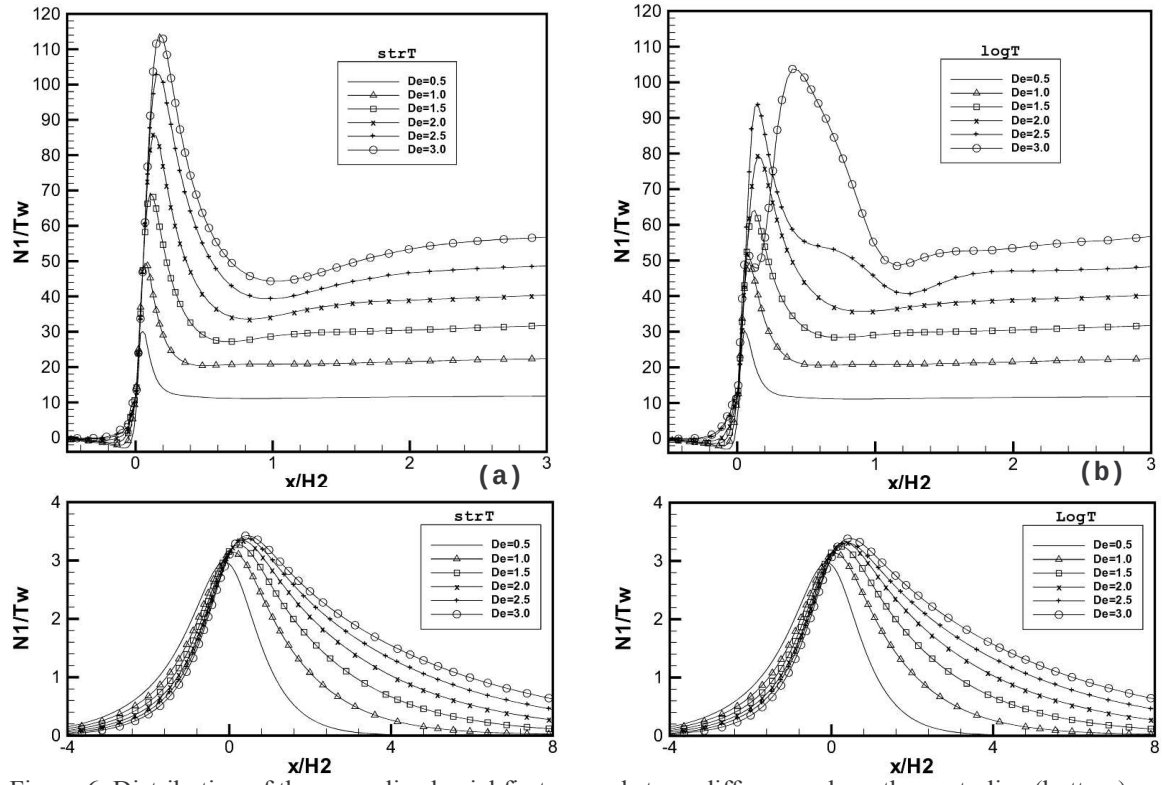

Figure 6. Distribution of the normalized axial first normal stress difference along the centreline (bottom) and near the downstream duct wall (top) in mesh M2 with CUBISTA - UCM: (a) *strT*; (b) *LogT*

Figure 5 shows maps of the various streamline patterns (in the top half of each contraction) together with flow classification maps (in the bottom half of each contraction) as function of Deborah number, obtained with both formulations on mesh M2. For each case the minimum values of the stability criteria, S_{min} and the det$(\mathbf{A})_{min}$, are presented. In the streamline flow maps, all trends are similar up to $De\approx2$. At higher Deborah numbers,

both the intensity of the corner vortex and its size are affected by the unsteady motion in the *LogT* simulations. This also happens in the flow classification maps: up to $De \approx 2$, the flow shows the demarked zones of rotation ($D \rightarrow -1$; points 1 and 2), of plane shear flow ($D \approx 0$; point 3) and of extensional flow ($D \rightarrow 1$, point 4). At $De \in [2.5,3]$ the differences between the two formulations in the lip vortex zone are clearly visible, with a small extensional cluster appearing, somehow suggesting that the formation and growth of the lip and corner vortices could be an extensional effect. In all simulations the minimum values of the stability criteria, S_{min} and the $\det(\mathbf{A})_{min}$, are positive, which indicate that there was no temporal loss of evolution at Deborah numbers up to $De=3$ (in simulations at higher *De* this is also true).

Finally, **Figure 6** presents the distribution of the normalized first normal stress difference along the centreline and near the downstream channel wall in mesh M2 with CUBISTA. The differences in the N_1/T_w in the axial direction, near the downstream duct wall at $De \approx 2.5$ and $De \approx 3$ in the *LogT* formulation simulations correlate well with information of **Figure 4** on the pulsation of the vortices. Note that the unsteady flow is not observed along the axial direction at $y/H_2=0$, i.e, along the centreline, its effect is only felt near the wall.

5.2 Oldroyd-B model

Results for the length of the corner vortex (X_R) for the Oldroyd-B model for both *strT* and *LogT* formulations are presented in **Table 3** and depicted in **Figure 7**.

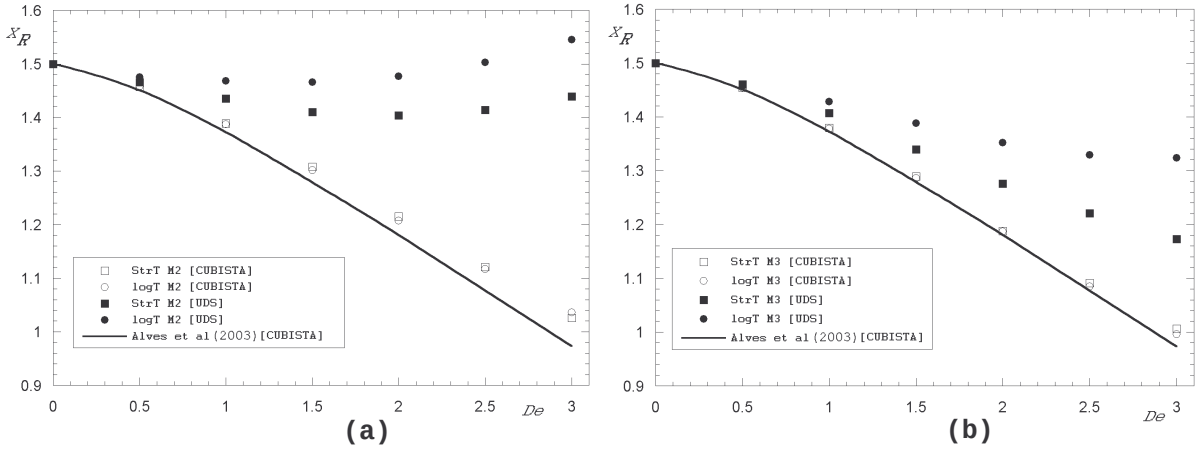

Figure 7. Dimensionless length of primary vortex as function of Deborah number: (a) M2; (b) M3 (Oldroy-B model).

		M1		M2		M3	
De	Scheme	***StrT***	***LogT***	***StrT***	***LogT***	***StrT***	***LogT***
0.0	Cubista	1.495	1.495	1.497	1.497	1.499	1.499
0.5	UDS	1.466	1.477	1.466	1.475	1.460	1.457
	Cubista	1.456	1.457	1.457	1.458	1.454	1.454
1.0	UDS	1.453	1.488	1.435	1.468	1.407	1.428
	Cubista	1.397	1.395	1.389	1.387	1.379	1.378
1.5	UDS	1.456	1.513	1.410	1.466	1.339	1.388
	Cubista	1.322	1.315	1.308	1.302	1.289	1.286
2.0	UDS	1.478	1.552	1.404	1.477	1.276	1.352
	Cubista	1.238	1.230	1.215	1.207	1.188	1.185
2.5	UDS	1.512	1.596	1.414	1.503	1.221	1.329
	Cubista	1.149	1.159	1.121	(1.117)[a]	1.091	(1.102)[a]
3.0	UDS	1.569	1.652	1.439	1.545	1.173	1.324
	Cubista	1.071	(1.056) [a]	1.026	(1.037)[a]	1.008	(1.065)[a]

Table 3. Dimensionless length of primary vortex (X_R) as a function of Deborah number, mesh, interpolating scheme and formulation (Oldroyd-B model).

Simulations with the QUICK scheme were also carried out, but for conciseness, they are not presented here. As for the UCM model, the results obtained with the Oldroyd-B model for both formulations follow the trends found in the literature, especially those from Alves et al [10], Aboubacar et al [19], Kim et al [20] and Belblidia et al [21], with the length of the corner vortex seen to decrease with elasticity up to a level of $De \approx 3$.

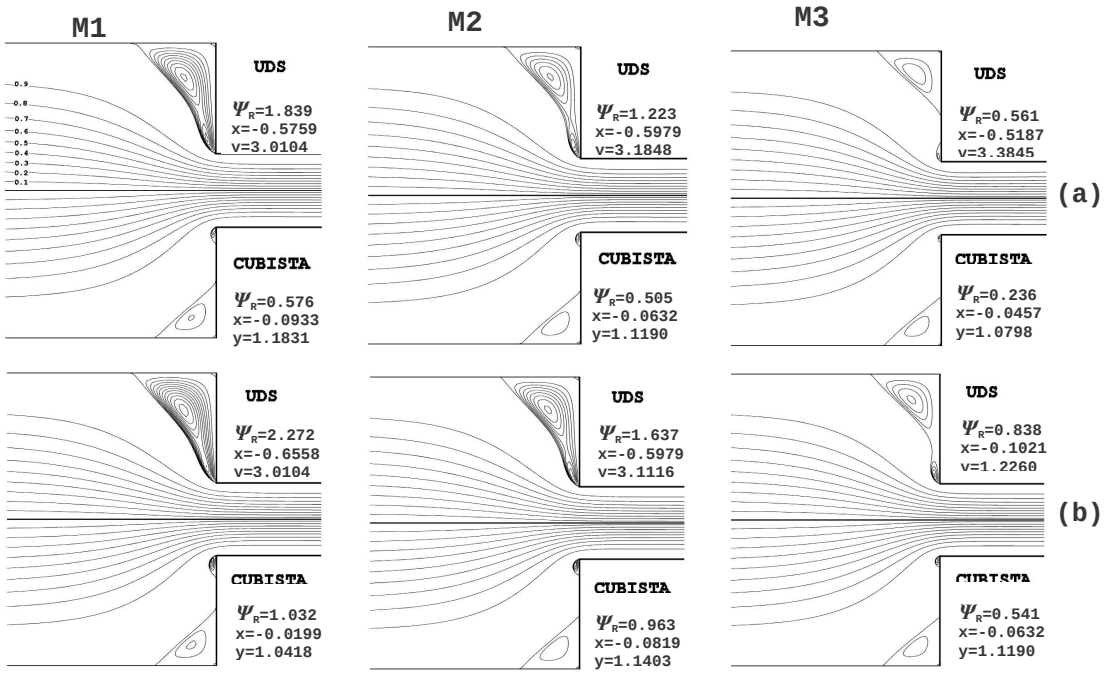

Figure 8. Coupled effect of mesh refinement and differencing scheme on the streamline patterns at De=2.5: (a) *strT*; (b) *LogT*. Note: $\Delta\Psi = 0.2 \times 10^{-3}$ in recirculations Ψ_R multiplied by 10^3 (Oldroyd-B model).

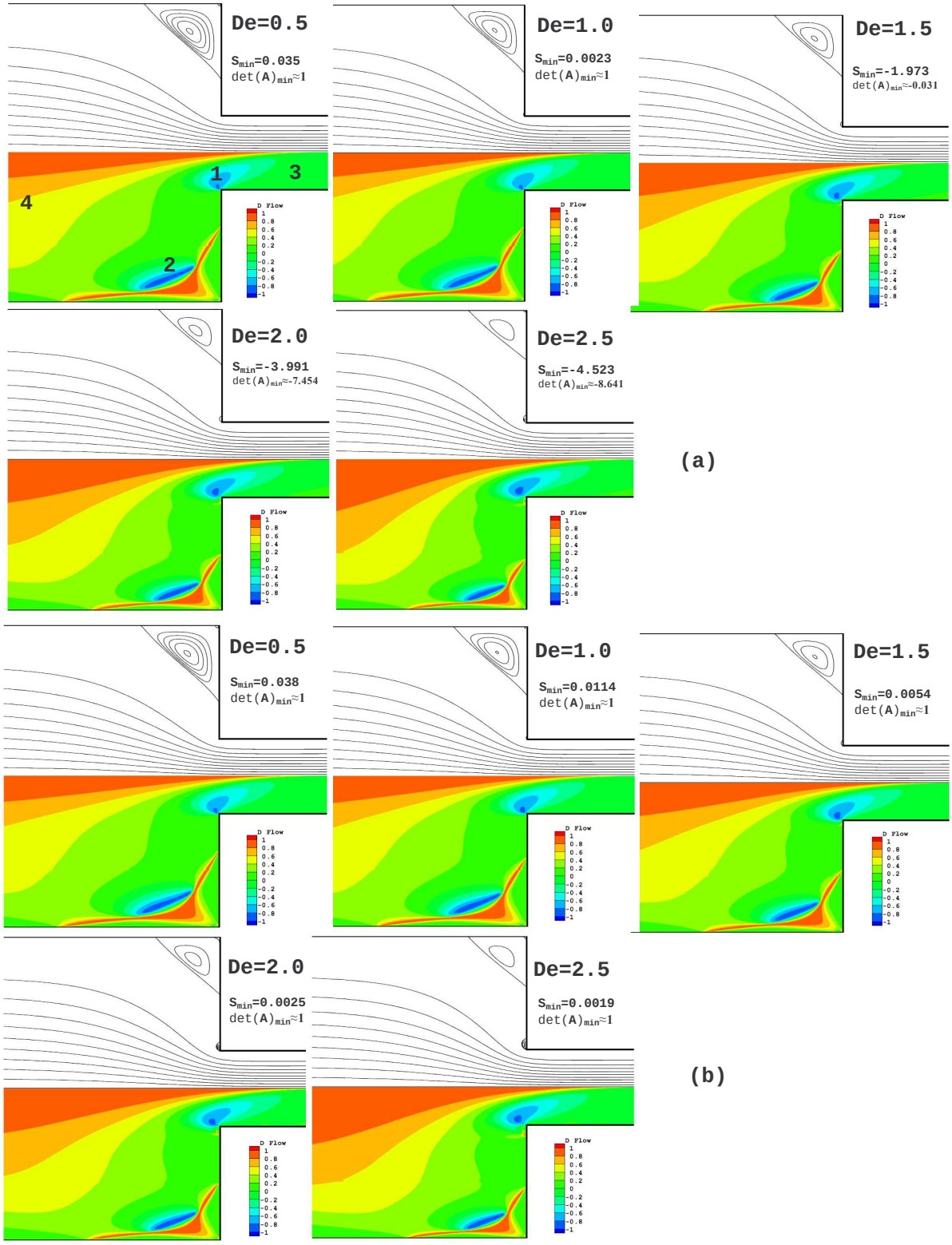

Figure 9. Flow patterns (top half) and flow classification (bottom half) on mesh M3 (Oldroyd-B model). (a) *strT*; (b) *LogT* [S_{min} and det(**A**)$_{min}$ – beside each map]

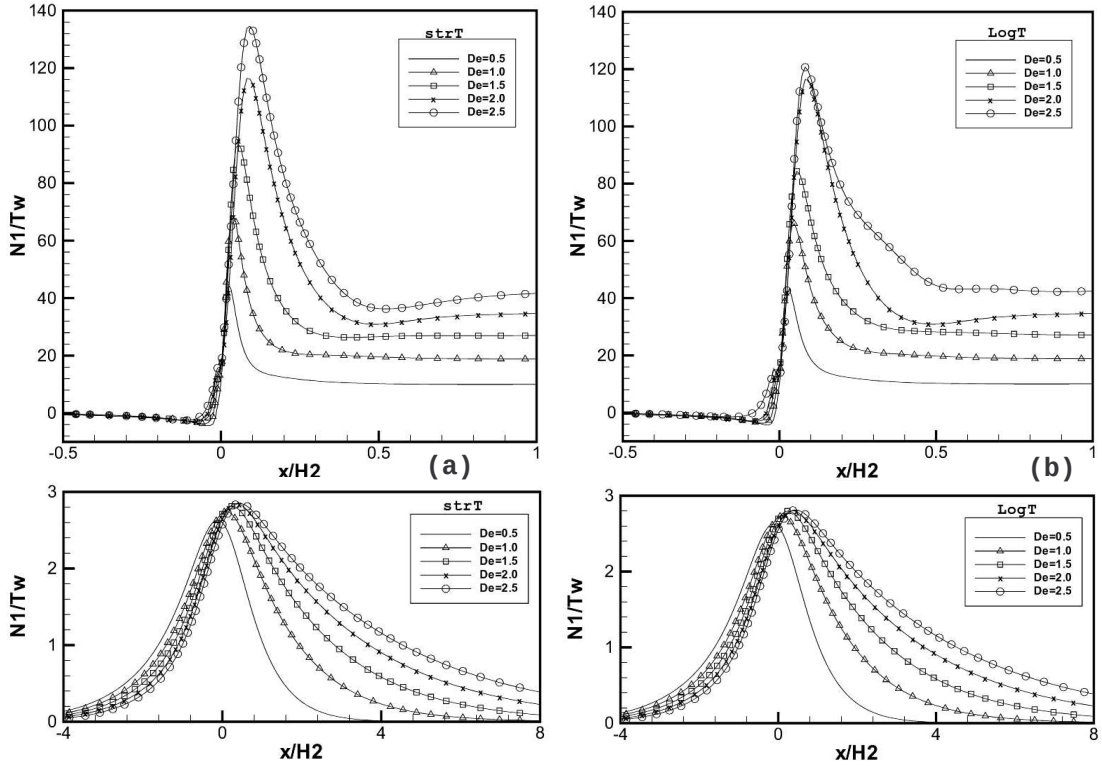

Figure 10 . Distribution of the normalized axial first normal stress difference along the centreline (bottom) and near the downstream duct wall (top) in mesh M3 with CUBISTA (Oldroyd-B model): (a) *strT*; (b) *LogT*

Once again, the *LogT* formulation is able to capture an instability, with the unsteady behaviour appearing at $De \approx 2.5$ on mesh M3 and $De \approx 3$ on mesh M2, when using the CUBISTA scheme. With the more diffusive UDS scheme, steady converged simulations were obtained up to $De=5.0$ on mesh M3 (at higher *De*, oscillations do start). The values of X_R inside brackets in **Table 2** represent the average value of X_R corresponding to this harmonic oscillation. Inspection of **Figure 8** and **9** allows us to conclude that the unsteady behaviour with the Oldroyd-B model is not only related with the merging of the two vortices, but with also with the formation and growth of the lip vortex. The limit of $De \approx 2.5$ with temporal oscillations is also reported in Aboubacar *et al* [21] with their finest mesh. **Figure 8** shows the coupled effect of mesh refinement and differencing scheme on the streamline patterns at $De=2.5$ and mesh M3, for both formulations. At this Deborah number simulations with the CUBISTA scheme in meshes M2 and M3 present periodically harmonic oscillations. All simulations with *LogT* result in higher values of Ψ_R than the *strT* simulations, but in both cases those values tend to decrease with mesh refinement. The eye of the recirculation is located in the same region for all formulations, schemes and meshes, except for the UDS simulation with the *LogT* formulation, changing from the salient corner zone to the re-entrant corner zone. The lip vortices in all *LogT* simulations are bigger than the *strT* counterparts. This feature is also confirmed in **Figure 9** with the streamline patterns (in the top symmetry plain of each *De* map) together with flow classification maps (in the bottom symmetry plain of each *De* map) as function of Deborah number obtained with both formulations in mesh M3. At Deborah numbers up to

De≈2, the trends of both formulations are similar. In contrast with the UCM model, the Oldroyd-B model simulations with the *strT* formulation presented some numerical degradation, with the minimum value of the stability criteria, S_{min} and the $\det(\mathbf{A})_{\min}$, becoming negative at *De*≈1.5, due probably to the lower $L_{2\text{-}norm}$ limit in these simulations. In the *LogT* simulations, both minimum stability criteria decrease with the increase of Deborah number, but are always positive, as postulated in [1-6], showing its strength for high Deborah number simulations. In the *D*-maps for the Oldroyd-B model, the three types of flow were clearly identified: the plane shear flow ($D \approx 0$; point 3) in the neighbourhood of the walls and elsewhere in the contraction zone; extensional flow ($D \rightarrow 1$, point 4) just before the contraction entrance and near the corner, and near rigid body flow in two demarked zones of rotation ($D \rightarrow -1$; points 1 and 2). As *De* increases, the dynamics of these zones also change (irrespective of formulation): rotation near the re-entrant corner increases and near the salient corner; extensional flow in the corner decreases and in the contraction entrance increases. An interesting aspect is the appearance of extensional flow in the lip vortex zone at high Deborah numbers with higher intensity for the *LogT* formulation. **Figure 10** presents the distribution of the normalized first normal stress difference along the centreline and near the downstream channel wall in mesh M3 with CUBISTA. As for the UCM model results, the unsteady features are only visible near the wall and are not observed in the axial direction, along the centreline.

6 CONCLUSIONS

A finite-volume method (FVM) was adapted to the log-conformation formulation of Fattal and Kupferman [1] and applied to the simulation of two dimensional laminar viscoelastic flow through a planar 4:1 abrupt contraction, using both the upper-convected Maxwell and Oldroyd-B models. In a strict sense, the Log conformation was not able to overcome the High Weissenberg Number Problem (HWNP), as claimed by other workers in the field who have applied it together with globally stable differential constitutive equations [1-5]. This apparent failure of achieving higher *De* numbers was traced back to the onset of a time-dependent instability near the re-entrant corner. Further simulations with an accurate time-dependent version of the code are deemed necessary to fully elucidate this point.

8 ACKNOWLEDGEMENTS

The authors acknowledge funding from FEDER and FCT through projects POCI/EQU/59256/2004, POCI/EQU/56342/2004 and POCI/EME/59338/2004.

REFERENCES

[1] R. Fattal and R. Kupferman, 2004, Constitutive laws of the matrix-logarithm of the conformation tensor, J. Non-Newtonian Fluid Mech. 123, 281-285.

[2] R. Fattal, R. Kupferman, Time-dependent simulation of viscoelastic flows at high Weissenberg number using the log-conformation representation. J. Non-Newtonian Fluid Mech., 126 (2005) 23–37

[3] M. A. Hulsen, R. Fattal and R. Kupferman, 2005, Flow of viscoelastic fluids past a cylinder at high Weissenberg number: Stabilized simulations using matrix logarithms, J. Non-Newtonian Fluid Mech. 127, 27-39.

[4] Y. Kwon, 2004, Finite element analysis of planar 4:1 contraction flow with the tensor-logarithmic formulation of differential constitutive equations, Korea-Australia Rheology J. 16, 183-191.

[5] S. Yoon and Y. Kwon, 2005, Finite element analysis of viscoelastic flows in a domain with geometric singularities, Korea-Australia Rheology J., 17, 99-110.

[6] J.G. Oldroyd, On the formulation of rheological equations of state Proc. R. Soc. Lond., A200 (1950) 523–541.

[7] Bird RB, Armstrong RC, Hassager O (1987) Dynamics of polymeric liquids, vol 1. Fluid mechanics, 2nd edn. Wiley, New York

[8] Oliveira PJ, Pinho FT. Plane contraction flows of Upper Convected Maxwell and Phan-Thien–Tanner fluids as predicted by a finite-volume method. J Non-Newt Fluid Mech. 1999;88:63-88.

[9] Alves MA, Pinho FT, Oliveira PJ. Effect of a high-resolution differencing scheme on finite-volume predictions of viscoelastic flows. J Non-Newt Fluid Mech. 2000;93:287-314.

[10] Alves MA, Oliveira PJ, Pinho FT. Benchmark solutions for the flow of Oldroyd-B and PTT fluids in planar contractions. J Non-Newt Fluid Mech. 2003;110:45-75.

[11] O. Hassager, Working Group on Numerical Techniques, in: Proceedings of the Vth Workshop on Numerical Methods in Non-Newtonian Flow, J. Non-Newtonian Fluid Mech. 29 (1988) 2–5.

[12] R.G. Owens, T.N. Phillips, Computational Rheology, Imperial College Press, London, 2002.

[13] McKinley, G.H., Raiford, W.P., Brown, R.A., and Armstrong, R.C., 1991, "Nonlinear Dynamics of Viscoelastic Flow in Axisymmetric Abrupt Contractions", J. Fluid Mech, Vol. 223, pp. 411-456.

[14] D.V. Boger, Viscoelastic flows through contractions, Ann. Rev. Fluid Mech. 19 (1987) 157–182.

[15] R. Keunings, Simulation of viscoelastic flow, in: C.L. Tucker (Ed.), Computer Modeling for Polymer Processing, Hanser, Munich, 1989, pp. 404–469.

[16] F.T.P. Baaijens, Mixed finite element methods for viscoelastic flow analysis: a review, J. Non-Newtonian Fluid Mech. 79 (1998) 361–385.

[17] K. Walters, M.F. Webster, The distinctive CFD challenges of computational rheology, ECCOMAS Swansea 2001, Int. J. Num. Meth. Fluids 45 (2003) 577–596.

[18] M. A. Alves, F. T. Pinho and P. J. Oliveira, Visualizations of Boger Fluid Flows in a 4:1 Square–Square Contraction, AIChE Journal, Vol. 51, No. 11, 2005

[19] Aboubacar, M.F. Webster, A cell-vertex finite volume/element method on triangles for abrupt contraction viscoelastic flows, 98 (2001) 83-106.

[20] J. M. Kim, C Kim, J H Kim, C Chung, K H Ahn, S J Lee, High-resolution finite element simulation of 4:1 planar contraction flow of viscoelastic fluid, J. Non-Newtonian Fluid Mech. 129 (2005) 23–37

[21] F. Belblidia, I.J. Keshtiban, M.F. Webster, Stabilised computations for viscoelastic flows under compressible implementations J. Non-Newtonian Fluid Mech., (2006) in preparation.

[22] Dupret F, Marchal JM (1986) Loss of evolution in the flow of viscoelastic fluids. J Non-Newtonian Fluid Mech 20:143–171

[23] Lee, J., S. Yoon, Y. Kwon and S.J. Kim, 2004, Practical comparison of differential viscoelastic constitutive equations in finite element analysis of planar 4:1 contraction flow. Rheol. Acta 44: 188–197

[24] G. Astarita, Objective and generally applicable criteria for flow classification, J. Non-Newtonian Fluid Mech. 6 (1979) 69–76.

[25] G. Mompean, R.L. Thompson, P.R. Souza Mendes, A general transformation procedure for differential viscoelastic models, J. Non-Newtonian Fluid Mech. 111 (2003) 151–174

[26] R.L. Thompson, P.R. S. Mendes, M.F. Naccache, A new constitutive equation and its performance in contraction flows J. Non-Newtonian Fluid Mech. 86 (1999) 375-388

[27] F. R. Phelan, S. D. Hudson and M. D. Handler, Fluid dynamics analysis of channel flow geometries for materials characterization in microfluidic devices, Rheol Acta (2005) 45: 59–71

[28] Oliveira PJ, Pinho FT, Pinto GA, Numerical simulation of non-linear elastic flows with a general collocated finite-volume method, J. Non-Newtonian Fluid Mech. 79 (1998) 1–43.

[29] M A Alves, P J Oliveira, F T Pinho, A convergent and universally bounded interpolation scheme for the treatment of advection, Int J Num Methods in Fluids, 41 (2003) 47.

[30] B.P. Leonard, A stable accurate convective modelling procedure based on quadratic upstream interpolation, Comput. Methods Appl. Mech. Eng. 19 (1979) 59–98.

[31] Oliveira, PJ, Time-dependent simulations of shear-thinning elastic flows through contractions, 2001, Proceedings of 2001 ASME - IMECE M.